Electronic structures of puckered bilayer group-V two-dimensional materials: Group theoretical analysis

メタデータ	
	言語: eng
	出版者:
	公開日: 2022-02-18
	キーワード (Ja):
	キーワード (En):
	作成者:
	メールアドレス:
	所属:
URL	https://doi.org/10.24517/00065294

The Japan Society of Applied Physics

Electronic structures of puckered bilayer group-V two-dimensional materials: group theoretical analysis

View the article online for updates and enhancements.

REGULAR PAPER

Electronic structures of puckered bilayer group-V two-dimensional materials: group theoretical analysis

Muhammad Yusuf Hakim Widianto[1][*] , Aflah Zaharo[1,2], Nuning Anugrah Putri Namari[1], and Mineo Saito[3]

[1]Graduate School of Natural Science and Technology, Kanazawa University, Kanazawa 920-1192, Japan
[2]Physics Department, Institute of Technology Bandung, Bandung 40132, Indonesia
[3]Faculty of Mathematics and Physics, Institute of Science and Technology, Kanazawa University 920-1192, Japan

[*]E-mail: mwidianto@cphys.s.kanazawa-u.ac.jp

We systematically study geometries and band structures of two-dimensional group-V bilayer materials, i.e. phosphorene, arsenene and antimonene. Among the four stacking structures (AA, AB, AC, and AD), the AB stacking structures are found to be the largest band gaps and to be the most energetically stable. We find novel band structures on the whole Brillouin zone edges: four bands have close energies and two of the four bands have the same energy in many cases. We analyze the characteristic features of the band structures based on the group theory and clarify that the features depend on the space group of each stacking structure. We also find that the band splits due to the interlayer interaction is very small and this interaction becomes large as atoms become heavy. © 2021 The Author(s). Published on behalf of The Japan Society of Applied Physics by IOP Publishing Ltd

1. Introduction

Group-V two-dimensional materials recently attracted scientific interests.[1–3] Whereas the Dirac cone characterizes electronic properties of group-IV materials,[4–8] group-V materials are semiconductors having band gaps and are useful for device applications in optoelectronics, spintronics and thermoelectrics.[9–12]

It was theoretically predicted that phosphorenes have higher band gaps than the black phosphorus crystal and the band gap decreases as the thickness of the films becomes large.[13] Later phosphorene was experimentally fabricated and it was confirmed that the observed band gap of the monolayer is larger than that of black phosphorous (0.3 eV).[14,15] As well as phosphorene, other group-V materials, arsenene,[16–19] antimonene,[19–21] and bismuthene,[12,19,22,23] have been studied.

Group-V two-dimensional materials form puckered (α) or six member ring (β) structures and the two structures have close energies.[19,24,25] Recently, the novelty of the monolayer forming α-structures was found; all the bands are doubly degenerated on the whole Brillouin zone edge and this degeneracy is explained based on the group theory.[19] Bilayer materials are expected to have different optical properties and thus clarification of the atomic geometries and band structures is necessary.

The purpose of this study is to systematically study the electronic and atomic structures of the α-structures of group-V bilayers. We perform first-principles density-functional-based calculations. We first optimize the geometries and clarify which stacking structure is the most stable. Next, we calculate the band structures and analyze them based on the group theory. We in particular focus on electronic band structures of the first Brillouin zone (FBZ) edge.

2. Method

We use slab models to simulate two-dimensional materials; a vacuum space of 20 Å in the z-axis is introduced to avoid the interaction between adjacent slabs (Fig. 1). We carry out density functional band structure calculations based on the generalized gradient approximation.[26,27] An ultrasoft pseudopotential[28] and norm-conserving pseudopotentials[29] are used for the Sb atom and for the other atoms, respectively. The cutoff energy of the wavefunctions is taken to be 30 Rydberg. We optimize the geometries under the condition that the atomic forces are less than 5×10^{-3} eV Å^{-1}.

We identify the irreducible representations (IR) for the calculated bands based on the group theory. The projection operator method is used for this identification, which was explained in previous papers.[19,30–32] This method is implemented in the first-principles calculation code, PHASE/0, and thus IR are identified automatically by using computers.[33] In this study, we adopt the Mulliken and Bethe symbols for the IR in most cases.[19,30–32,34,35] However, in some exceptional cases, IR do not correspond to conventional IR as mentioned in the next section. In this nonconventional case, we use other symbols.

3. Results and discussion

3.1. Optimized structure

3.1.1. Phosphorene. We first optimize the lattice constants and internal atomic coordinates of monolayer phosphorene (Table I). Four atoms are in the unit cell shown in Fig. 1(a). We find that the two top atoms are not buckled (Fig. 1) and thus the system belongs to $Pmna$ (D_{2h}^{7}), which is one of the non-symmorphic space groups (all the systems studied in this paper belong to non-symmorphic space groups). The bond length of the horizontal two top atoms (r_1) is 2.24 Å and the vertical bond length connecting the top and bottom atoms (r_2) is 2.25 Å (Fig. 1). The calculated two bond angles, θ_1 and θ_3, defined in Fig. 1, are 103.3° and 97.8°, respectively. These bond angles (θ_1 and θ_3) are rather close to the sp^3 angle (109.5°) due to the fact that the P atom favors sp hybridization.[13]

We next study bilayers of phosphorene and consider four possible stacking structures, i.e. AA, AB, AC, and AD (Fig. 2).[36] We find that the non-buckled structures are stable for all the stackings. In the AA stacking structure, the second
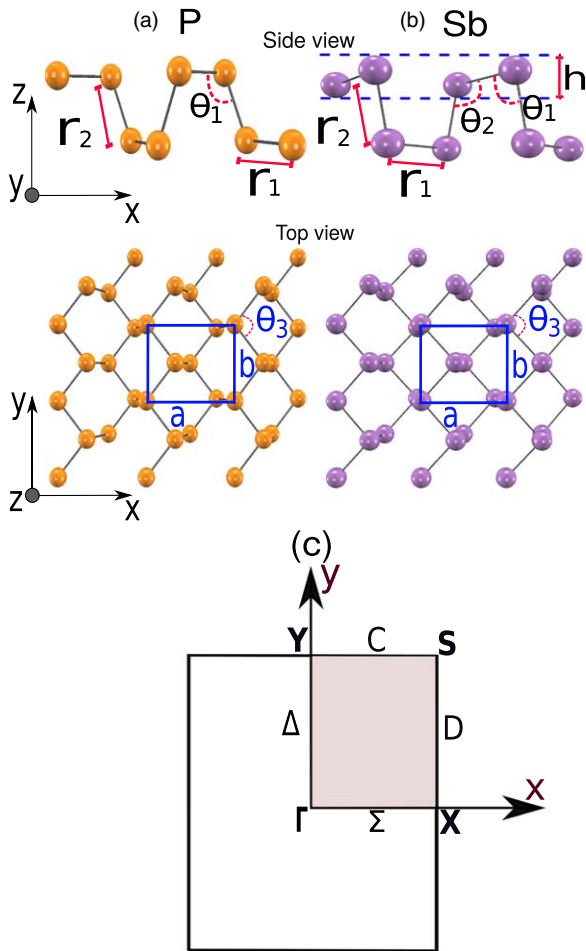
Fig. 1. (Color online) Atomic structures of the monolayer phosphorene (a) and antimonene (b) and the FBZ (c).

layer is directly stacked on the top of the first layer and thus the structure belongs to $Pmna$ (D_{2h}^7) which is the same as the space group of the monolayer. The AB stacking structure is generated by shifting the second layer by ½ of the lattice period along the x-axis (or y-axis), which is the same as the stacking in black phosphorus. The space group in the AB stacking structure is $Pbcm$ (D_{2h}^{11}). The AC (AD) stacking structure is generated by rotating 180° in the z-axis of the second layer in the AA (AB) stacking, and as a result, the space group belongs to $Pnma$ (D_{2h}^5)

and $Pccm$ (D_{2h}^3) for the AC and the AD stacking structures, respectively. We optimize the lattice constants and find that the difference among the lattice constants of the monolayer and bilayer structures is rather small (Table I) and the values are close to experimental values of crystals ($a = 4.40$ Å and $b = 3.40$ Å).[13]

The layer distance (d) is found to be 4.25 Å, 4.34 Å, 4.18 Å, and 4.32 Å for the AA, AB, AC, and AD stacking structures, respectively (Table I). These values are much longer than the bond lengths (r_1 and r_2), therefore the interaction between the two layers is rather weak, which leads to the fact that the optimized lattice constants of mono- and bi-layers are close (Table I). Furthermore, the bond angles (θ_1 and θ_3) and bond lengths in the four stackings are close to those of the monolayer structure (Table I): the difference in bond lengths and bond angles are less than 0.06 Å and 2°, respectively.

We here calculate the cohesive energy of the bilayer structures to clarify the stability of each stacking structure. The cohesive energy is given by

$$E_{\text{cohesive}} = \frac{(nE_{\text{atom}} - E_{\text{bilayer}})}{n}.$$

In this expression, E_{atom} and n are the total energy of an isolated single atom and the number of atoms in a single supercell, respectively. E_{bilayer} is the total energy of the bilayer. We find that the AB stacking structure is the most stable among the four stacking structures: the cohesive energy is about 10 meV/atom higher than those of AA, AC, and AD stacking structures (Table II).

3.1.2. Arsenene. We find that two top atoms of the arsenene monolayer are not buckled as in the case of phosphorene and the symmetry belongs to $Pmna$ (D_{2h}^7) which is the same as that of phosphorene. The bilayer AA, AB, AC, and AD stacking structures also form non-buckled structures and thus the space groups are the same as those in phosphorene, i.e. AA, AB, AC, and AD stacking structures belong to $Pmna$ (D_{2h}^7), $Pbcm$ (D_{2h}^{11}), $Pnma$ (D_{2h}^5), and $Pccm$ (D_{2h}^3), respectively.[36] The AB stacking structure is the most stable as in the case of phosphorene and its cohesive energy is 2–9 meV/atom higher than the other three stacking structures (Table II). The layer distance (d) is found to be 4.08 Å, 4.10 Å, 4.02 Å, and the 3.98 Å for AA, AB, AC, and

Table I. Lattice constants and optimized geometries of mono- and bi-layers forming AA, AB, AC and AD stacking structures. The bond lengths (r_1 and r_2), layer distance between two layers (d), buckling amplitude (h) and bond angles (θ_1, θ_2 and θ_3) are defined in Fig. 1. The units of the bond angles are degree.

System	Stacking	a (Å)	b (Å)	r_1 (Å)	r_2 (Å)	d (Å)	h (Å)	θ_1	θ_2	θ_3
P	Monolayer	4.52	3.38	2.24	2.25	—	—	102.8	—	96.8
	AA	4.60	3.32	2.23	2.26	4.25	—	103.9	—	96.3
	AB	4.61	3.32	2.27	2.31	4.34	—	102.9	—	94.7
	AC	4.60	3.32	2.23	2.26	4.18	—	103.9	—	94.8
	AD	4.60	3.32	2.23	2.26	4.32	—	104.0	—	96.3
As	Monolayer	4.76	3.68	2.51	2.50	—	—	100.5	—	94.2
	AA	4.78	3.62	2.50	2.51	4.08	—	100.5	—	94.1
	AB	4.80	3.60	2.51	2.50	4.10	—	100.6	—	94.3
	AC	4.79	3.60	2.51	2.49	4.02	—	100.6	—	94.2
	AD	4.77	3.61	2.52	2.49	3.98	—	100.6	—	94.3
Sb	Monolayer	4.73	4.29	2.92	2.84	—	0.42	87.8	104.0	94.6
	AA	4.62	4.30	2.90	2.92	3.35	0.26	89.8	100.5	95.4
	AB	4.72	4.30	2.91	2.86	3.49	0.30	90.2	102.1	94.8
	AC	4.57	4.32	2.93	2.87	3.24	0.32	88.3	101.1	94.7
	AD	4.69	4.31	2.92	2.86	3.21	0.31	90.1	102.0	94.5
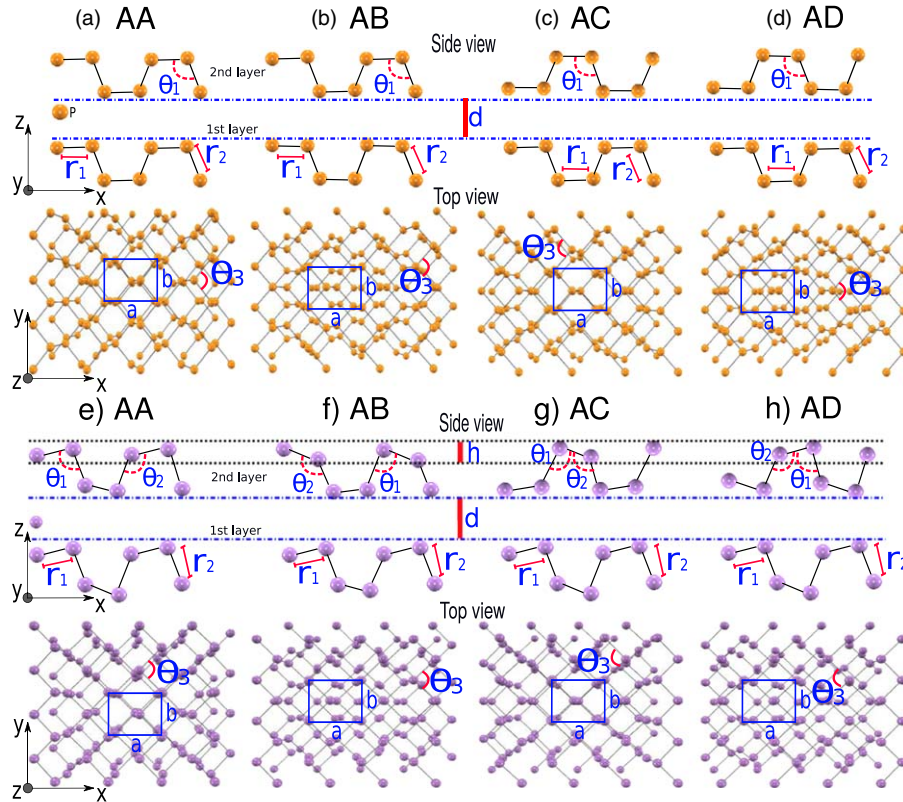
Fig. 2. (Color online) Bilayer of the AA, AB, AC, and AD stackings. Phosphorenes and antimonenes are presented in the upper and lower parts, respectively. The bond lengths (r_1 and r_2), bond angles (θ_1, θ_2 and θ_3), buckling amplitudes (h) and layer distance (d) are tabulated in Table I.

Table II. Cohesive energies ($E_{cohesive}$) and band gaps (E_g) for mono- and bi-layers forming AA, AB, AC and AD stacking structures.

System	Stacking	$E_{cohesive}$ (eV/atom)	E_g (eV)
P	Monolayer	0.885	0.90
	AA	0.893	0.49
	AB	0.901	0.54
	AC	0.891	0.33
	AD	0.893	0.35
As	Monolayer	2.310	0.80
	AA	2.319	0.11
	AB	2.321	0.30
	AC	2.312	0.10
	AD	2.316	0.18
Sb	Monolayer	7.532	0.34
	AA	7.557	Metallic
	AB	7.569	Metallic
	AC	7.555	Metallic
	AD	7.554	Metallic

AD stacking structures, respectively (Table I). These values are smaller than the corresponding values of phosphorene whereas the bond lengths (r_1 and r_2) are larger than those in phosphorene. These results indicate that the interlayer interaction is somewhat stronger than that in phosphorene.

3.1.3.   Antimonene. We optimize the geometry of the monolayer antimonene and find that the two top atoms are buckled and this buckling leads to the space group of $Pmn2_1$ (C_{2v}^7) which is lower than that of monolayer phosphorene and arsenene. Four atoms are in the unit cell shown in Fig. 1(b). The buckling amplitude (h) defined in Fig. 1 is 0.42 Å and this buckling is expected to be due to the electron transfer from the higher-position atom to lower-position atom as was

discussed in previous studies.[13,19] The calculated bond lengths and bond angles are tabulated in Table I.

We next study four types of stacking structures (AA, AB, AC, and AD). Two top atoms are found to be buckled for all four structures. The AB stacking structure is found to be the most stable among the four stacking structures (Table II). The layer distances (d) for the AA, AB, AC, and AD stacking structures are found to be 3.35 Å, 3.49 Å, 3.24 Å, and 3.21 Å, respectively. These values are much longer (10%–20%) than those of the bond lengths (r_1 and r_2), indicating that the interaction between the two layers is weak. However, these values are smaller than those in phosphorene and arsenene, which indicates that the interlayer interaction is stronger than those in phosphorene and arsenene. We find that the bond lengths in the bilayers are close to those of the monolayer; the maximum difference is 0.07 Å. The geometries of AA, AB, AC, and AD stacking structures belong to the space groups, $Pmn2_1$ (C_{2v}^7), $Pmn2_1$ (C_{2v}^7), $P2_1/m$ (C_{2h}^2), and $P2_1/m$ (C_{2h}^2), respectively. These space groups are lower than those in the non-buckled structures.

3.2.   Band structures of bilayers analyzed based on the group theory

We here calculate electronic band structures. Conventional IR are denoted by using Bethe and Mulliken symbols in Table III. In some cases, IR are different from the conventional ones on some parts of FBZ edges because the present systems are non-symmorphic. In these nonconventional cases, we use symbols consisting of the k point and suffixes in Tables IV and V. At the k point X for example, we use symbols of X_n and $X_n^\pm$, where n is the number assigned to each IR and the signs ± represent the parity when the k group includes the inversion symmetry. These symbols are simply

Table III. Character table for the conventional IR. We use Bethe symbols and the corresponding Mulliken symbols in the parentheses.

Point group	IR	E	$C_2(x)$	$C_2(y)$	$C_2(z)$	IE	σ_{yz}	σ_{xz}	σ_{xy}
D_{2h}	Γ_1^+ (A_g)	1	1	1	1	1	1	1	1
	Γ_1^- (A_u)	1	1	1	1	-1	-1	-1	-1
	Γ_2^+ (B_{1g})	1	1	-1	-1	1	1	-1	-1
	Γ_2^- (B_{1u})	1	1	-1	-1	-1	-1	1	1
	Γ_3^+ (B_{2g})	1	-1	1	-1	1	-1	1	-1
	Γ_3^- (B_{2u})	1	-1	1	-1	-1	1	-1	1
	Γ_4^+ (B_{3g})	1	-1	-1	1	1	-1	-1	1
	Γ_4^- (B_{3u})	1	-1	-1	1	-1	1	1	-1
C_{2v}	Γ_1 (A_1)	1	1					1	1
	Γ_2 (A_2)	1	1					-1	-1
	Γ_3 (B_1)	1	-1					1	-1
	Γ_4 (B_2)	1	-1					-1	1
C_{2h}	Γ_1^+ (A_g)	1		1		1		1	
	Γ_1^- (A_u)	1		1		-1		-1	
	Γ_2^+ (B_g)	1		-1		1		-1	
	Γ_2^- (B_u)	1		-1		-1		1	
C_s	Γ_1 (A')	1						1	
	Γ_2 (A'')	1						-1	
C_2	Γ_1 (A)	1		1					
	Γ_2 (B)	1		-1					

Table IV. Character table of nonconventional IR for the non-buckled bilayer structure. The IR are represented by symbols consisting of k point and suffixes.

Stacking	k point	IR	E	$C_2(x)$	$C_2(y)$	$C_2(z)$	IE	σ_{yz}	σ_{xz}	σ_{xy}
AA, AB	$X(D_{2h})$	X_1	2	0	0	0	0	0	2	0
		X_2	2	0	0	0	0	0	-2	0
	$D(C_{2v})$	D_1	2		0			0		0
AA	$S(D_{2h})$	S_1^+	2	0	0	0	2	0	0	0
		S_1^-	2	0	0	0	-2	0	0	0
	$C(C_{2v})$	C_1	2	0					0	0
	$Y(D_{2h})$	Y_1	2	0	2	0	0	0	0	0
		Y_2	2	0	-2	0	0	0	0	0
AB	$S(D_{2h})$	S_1	2	2	0	0	0	0	0	0
		S_2	2	-2	0	0	0	0	0	0
	$Y(D_{2h})$	Y_1	2	0	0	0	0	0	0	-2
		Y_2	2	0	0	0	0	0	0	2
AC, AD	$X(D_{2h})$	X_1^+	1	1	$-i$	$-i$	$-i$	$-i$	1	1
		X_1^-	1	1	$-i$	$-i$	i	i	-1	-1
		X_2^+	1	1	i	i	$-i$	$-i$	-1	-1
		X_2^-	1	1	i	i	i	i	1	1
		X_3^+	1	-1	$-i$	i	$-i$	i	1	-1
		X_3^-	1	-1	$-i$	i	i	$-i$	-1	1
		X_4^+	1	-1	i	$-i$	$-i$	i	-1	1
		X_4^-	1	-1	i	$-i$	i	i	1	-1
	$D(C_{2v})$	D_1	1		$-i$			$-i$		1
		D_2	1		$-i$			i		-1
		D_3	1		i			$-i$		-1
		D_4	1		i			i		1
AC	$S(D_{2h})$	S_1	2	0	0	0	0	0	0	2
		S_2	2	0	0	0	0	0	0	-2
	$Y(D_{2h})$	Y_1	2	0	0	0	0	0	0	-2
		Y_2	2	0	0	0	0	0	0	2
AD	$S(D_{2h})$	S_1	2	0	$-2i$	0	0	0	0	0
		S_2	2	0	$2i$	0	0	0	0	0
	$C(C_{2v})$	C_1	2	0					0	0
	$Y(D_{2h})$	Y_1	2	0	2	0	0	0	0	0
		Y_2	2	0	-2	0	0	0	0	0

denoted by n and $n^\pm$, respectively, in the band figures (Figs. 3–5). As for the conventional IR, Bethe symbols, Γ_n and $\Gamma_n^\pm$, are used in Table III, where the signs ± represent parity, and are simply denoted by $\overset{*}{n}$ and $\overset{*}{n}{}^\pm$, respectively, in the band figures (Figs. 3–5) [the stars on n are used (not used) to represent the Bethe (nonconventional) symbols].

Band structures of monolayer puckered structures were previously reported and all the bands were doubly degenerated on the whole FBZ.[19] In this study, we focus on band structures of bilayer puckered structures.

3.2.1.   Phosphorene. We here calculate the band structures of bilayer AA, AB, AC, and AD stacking structures

Table V. Character table of nonconventional IR for the buckled bilayer structure. The IR are represented by symbols consisting of k point and suffixes.

Stacking	k point	IR	E	$C_2(x)$	σ_{xz}	σ_{xy}
AA	$S(C_{2v})$	S_1	2	0	0	0
	$C(C_{2v})$	C_1	2	0	0	0
	$Y(C_{2v})$	Y_1	2	0	0	0
		IR	E	$C_2(y)$	IE	σ_{xz}
AC, AD	$X(C_{2h})$	X_1^+	1	$-i$	$-i$	1
		X_1^-	1	$-i$	i	-1
		X_2^+	1	i	$-i$	-1
		X_2^-	1	i	i	1
	$D(C_2)$	D_1	1	$-i$		
		D_2	1	i		
AC	$S(C_{2h})$	S_1	2	0	0	0
	$Y(C_{2h})$	Y_1	2	0	0	0
AD	$S(C_{2h})$	S_1^+	1	$-i$	$-i$	1
		S_1^-	1	$-i$	i	-1
		S_2^+	1	i	$-i$	-1
		S_2^-	1	i	i	1

(Fig. 3). In all the four stacking structures, the Γ point belongs to D_{2h} and the point group includes eight symmetry operations (see Table VII).

We start to study band structure of the AA stacking structure [Fig. 3(a)]. In the whole band structures, two bands have very close energies or identical energy. For example, the lowest band and second lowest one at the Γ point belong to Γ_1^+ (A_g) and Γ_4^- (B_{3u}), respectively, and the energy difference is only 13 meV. These close energies originate from the fact that the interaction between the two layers are very weak and thus the energy split due to the interlayer interaction is very small. This weak interaction is due to the fact that the layer distance between the two layers is much longer than the bond lengths as was mentioned in the previous section.

Each two bands at the X point have the same energy whereas the two bands have different energies on the Σ line due to the fact that the two bands belong to different IR. This double degeneracy at the X point is caused by the fact that the two bands belong to nonconventional two-dimensional IR (X_1 or X_2), which are different from conventional IR because of the fact that the present system is non-symmorphic.[31] Two sets of the doubly degenerated bands have close energies. For example, in the lowest energy part, the energy split between the two X_1 states is 6 meV [In Fig. 3(a), the four bands seem to be merged because of the small energy split of 6 meV)].

We find that the band on the whole FBZ edges belong to nonconventional two-dimensional IR so that these bands are doubly degenerated; The IR on the D–S–C–Y line are denoted by D_1, S_1^+, S^{-1}, C_1, Y_1 and Y_2 (see Table IV). Two sets of the doubly degenerated bands have close energies since the energy split due to the interlayer interaction is weak [Fig. 3(a)].

We next study band structure of the AB stacking structure [Fig. 3(b)]. The four bands on the whole FBZ have close energies and two of the four bands have the same energy as in the case of the AA stacking structure (Table IV). The reason for this characteristic feature in the band structures is the same that in the case of AA stacking structure [Fig. 3(a)] except for the C line; whereas the bands belong to nonconventional two-dimensional IR in the case of the AA stacking, all the bands belong to conventional one-dimensional IR [Γ_1 (A_1), Γ_2 (A_2), Γ_3 (B_1),

and Γ_4 (B_2)] in the case of the AB stacking and pairing of bands induces double degeneracy: Γ_1 (A_1) [Γ_2 (A_2)] is paired with Γ_4 (B_2) [Γ_3 (B_1)] as Table VI shows. This pairing is due to the time-reversal symmetry as was discussed in a previous paper.[31]

We now study the band structure of the AC stacking structure (Fig. 3(c)). Four bands on the X–D line have close energies but each band has a different energy, i.e. there is no degeneracy on the X–D line. This feature is in sharp contrast with that in the AA and AB stacking structures, two bands have the same energy. The four different energies are due to the fact that four bands belong to the nonconventional one-dimensional IR (Table IV). On the S–C–Y line, each two bands are doubly degenerated. This is due to the fact that the bands at the S and Y points belong to nonconventional two-dimensional IR and bands on the C line belong to conventional one-dimensional IR which are paired due to the time-reversal symmetry (Tables IV and VI).

In the case of the AD stacking structure, bands on the X–D line belong to nonconventional one-dimensional IR and thus each band has a different energy (Table IV). Bands on the S–C–Y line belongs to nonconventional two-dimensional IR (Table IV) and thus the bands are doubly degenerated.

Our calculational results suggest that the monolayers and the bilayers are direct gap semiconductors, i.e. both the conduction band bottom and the valence band top are located at the Γ point (We have checked only k points which appear in the band figures [Figs. 3(a)–3(d)].). The direct gaps were also confirmed by previous studies.[36] We find that the AB stacking structure, which is found to be the energetically most stable, has the largest band gap. The band gaps of the four types of bilayers (0.33–0.54 eV) are lower than that of the monolayer (0.9 eV) as Table II shows.

3.2.2. Arsenene. We next study the arsenene bilayer forming AA, AB, AC, and AD stacking structures. Overall, the characteristic features in band structures are similar to those of phosphorene [Figs. 4(a)–4(d)]. This is because the space groups are the same as those in the case of phosphorene. However, we find that the band energy splits are generally larger than those in phosphorene (Figs. 3 and 4). This is because the interlayer interaction is somewhat stronger than that in the case of phosphorene as was discussed in 3.1.2: the layer distance in arsenene is smaller than that in phosphorene (Table I).

Our calculations suggest that the monolayer and four kinds of bilayers are direct gap semiconductors where both the conduction band bottom and valence band top are located at the Γ point [We have checked only on k points, which appear in the band figures Figs. 4(a)–4(d).]. The direct band gaps were also confirmed in previous studies.[19,37] The AB stacking structure, which is the energetically most stable, has the largest band gap and the bilayer band gaps (0.10–0.30 eV) are smaller than that of the monolayer (0.80 eV).

3.2.3. Antimonene. We now study the band structure of the antimonene bilayer forming AA, AB, AC, and AD stacking structures. We find that the symmetries of the AA and AB (AC and AD) stacking structures belong to C_{2v} (C_{2h}) at the Γ point. Four symmetry operations are included in this group (Table VII).

We start from the AA stacking structure [Fig. 5(a)]. The energy split between the first and second lowest bands at the
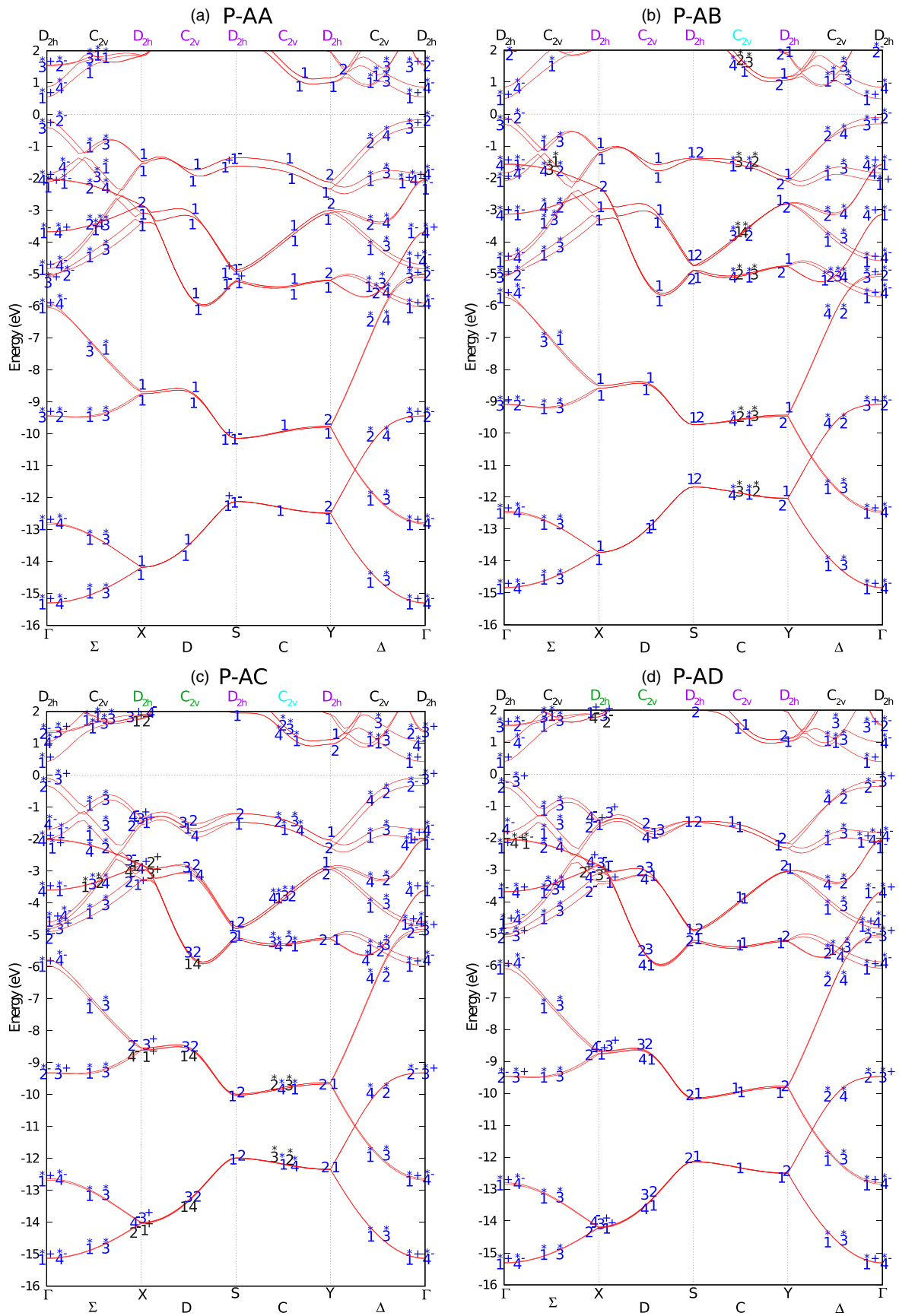
Fig. 3. (Color online) Band structures of bilayer phosphorene forming (a) AA, (b) AB, (c) AC and (d) AD stacking structures. Conventional IR are denoted by stars (*) and the nonconventional IR are represented without using stars. The characters of these IR are tabulated in Tables III and IV.

Table VI. Pairing of bands due to time-reversal symmetry. The Bethe symbols and the corresponding Mulliken symbols in the parentheses are presented.

System	Stacking	k point	Pairing
Non-buckled	AB, AC	$C(C_{2v})$	Γ_1 (A$_1$) [Γ_4 (B$_2$)]
			Γ_2 (A$_2$) [Γ_3 (B$_1$)]
Buckled	AA, AB	$X(C_{2v})$	Γ_1 (A$_1$) [Γ_3 (B$_1$)]
			Γ_2 (A$_2$) [Γ_4 (B$_2$)]
		$D(C_s)$	Γ_1 (A$'$) [Γ_2 (A$''$)]
	AB	$S(C_{2v})$	Γ_1 (A$_1$) [Γ_3 (B$_1$)]
			Γ_2 (A$_2$) [Γ_4 (B$_2$)]
	AC	$C(C_s)$	Γ_1 (A$'$) [Γ_2 (A$''$)]

Γ point is 280 meV, which is much larger than the values of phosphorene (13 meV) and arsenene (70 meV). This large energy split is expected to be due to the fact that the interlayer interaction is large compared with phosphorene and arsenene. The layer distance is 22%–27% smaller than that in the cases of arsenene and phosphorene. Overall on the FBZ edge, the splits of the bands are larger than those in phosphorene and arsenene.

On the whole FBZ edge, the bands are doubly degenerated: on the X–D line, pairing of the conventional one-dimensional IR occurs (Table VI) and the bands on the S–C–Y line belongs to nonconventional two-dimensional IR [Table V and Fig. 5(a)].

We now study the band structure of the AB stacking structure [Fig. 5(b)]. The bands are doubly degenerated on the X–D–S line due to the pairing of conventional one-dimensional IR (Table VI). On the contrary, each band has a different energy because the bands belong to conventional one-dimensional IR on the C–Y line (Table III).

In the case of the AC stacking structure, the four bands on the X–D line have different energies because the bands belong to nonconventional one-dimensional IR (Table V). On the contrary, the bands on the S–C–Y line are doubly degenerated because the bands at the S and Y points belong to nonconventional two-dimensional IR and the bands on the C line belong to conventional one-dimensional IR which are paired (Tables V and VI).

We next study the AD stacking structure. On the whole FBZ edge (X–D–S–C–Y), four bands have different energies because the bands belong to conventional or nonconventional one-dimensional IR (Tables III and V).

We find that the four bilayer stacking structures of antimonene are metallic. The conduction band bottom and the valence band top crossing the Fermi level at several points in the FBZ (Fig. 5). The other calculations including the hybrid-DFT and SOC also show that the band gap of bilayers antimonene is metallic and it is confirmed by the

experimental study that detects a metallic density of state on the bilayer cases.[38–40] Meanwhile, the monolayer structure is a direct gap semiconductor and the band gap is 0.34 eV as Table II shows.[19]

3.2.4. Summary of bands on FBZ edges of bilayers.
We have found that four bands on the FBZ edges have close energies and found four patterns;
(a) Two bands have the same energy due to sticking of nonconventional two-dimensional IR.
(b) Two bands have the same energy due to pairing of conventional one-dimensional IR.
(c) Four bands have different energies due to nonconventional one-dimensional IR.
(d) Four bands have different energies due to conventional one-dimensional IR.

For the symbols of k point groups in the band figures (Figs. 3–5), we use purple, cyan, green and red colors in the cases of (a)–(d), respectively.

In the AA stacking structure whose space group is the same as that of the monolayer, the degeneracy tends to occur. In the AC and AD stacking structures, the band splits become prominent compared with the AA and AB stacking structures. These features for the difference among the four stacking originate from the difference in the space group.

The energy split due to the interlayer interaction is found to be small. We find that the split becomes large as the atom becomes heavy.

We expect that the novel features of the band structures found in this study will be detected by using some experiments, for example, photoelectron spectroscopy.

4. Conclusion

We have carried out density functional band structure calculations of bilayer system group-V materials: phosphorene, arsenene and antimonene. We first clarify that the most stable structures among the bilayer stacking structures (AA, AB, AC, and AD) are the AB stacking structures. In general, the bond lengths are found to be smaller than the layer distance, indicating that the interlayer interaction is weak. This fact leads to small splitting of the bands due to the interlayer interaction. We find that the split increases as the atom becomes heavy.

All the monolayers are direct gap semiconductors and the phosphorene and arsenene bilayers are also direct gap semiconductors whereas the antimonene bilayers are found to be metallic. We find degeneracies on the whole or a part of FBZ edges and this degeneracy is analyzed based on the group theory: the degeneracies originate from pairing of conventional one-dimensional IR or from nonconventional two-dimensional IR. We find that the difference in features of

Table VII. Symmetry operations. Some operations include the fractional translation $\vec{\tau}_1 = \frac{1}{2}\vec{a} + \frac{1}{2}\vec{b} + \alpha\vec{c}$ and $\vec{\tau}_2 = \frac{1}{2}\vec{a} + \alpha\vec{c}$, where $\vec{a}$, $\vec{b}$, and $\vec{c}$ are the primitive lattice vectors in the x, y, and z directions, respectively, and the value of α is constant which depends on the value of c.

System	Stacking	Space group	Symmetry operation
Non-Buckled	AA	Pmna (D_{2h}^7)	$\{E\|0\}$, $\{C_2(x)\|\vec{\tau}_1\}$, $\{C_2(y)\|\vec{\tau}_1\}$, $\{C_2(z)\|\vec{\tau}_1\}$, $\{IE\|\vec{\tau}_1\}$, $\{\sigma_{yz}\|\vec{\tau}_1\}$, $\{\sigma_{xz}\|0\}$, $\{\sigma_{xy}\|\vec{\tau}_1\}$
	AB	Pbcm (D_{2h}^{11})	
	AC	Pnma (D_{2h}^5)	
	AD	Pccm (D_{2h}^3)	
Buckled	AA, AB	Pmn2$_1$ (C_{2v}^7)	$\{E\|0\}$, $\{C_2(x)\|\vec{\tau}_2\}$, $\{\sigma_{xz}\|0\}$, $\{\sigma_{xy}\|\vec{\tau}_2\}$
	AC, AD	P2$_1$/m(C_{2h}^2)	$\{E\|0\}$, $\{C_2(y)\|\vec{\tau}_1\}$, $\{IE\|\vec{\tau}_1\}$, $\{\sigma_{xz}\|0\}$
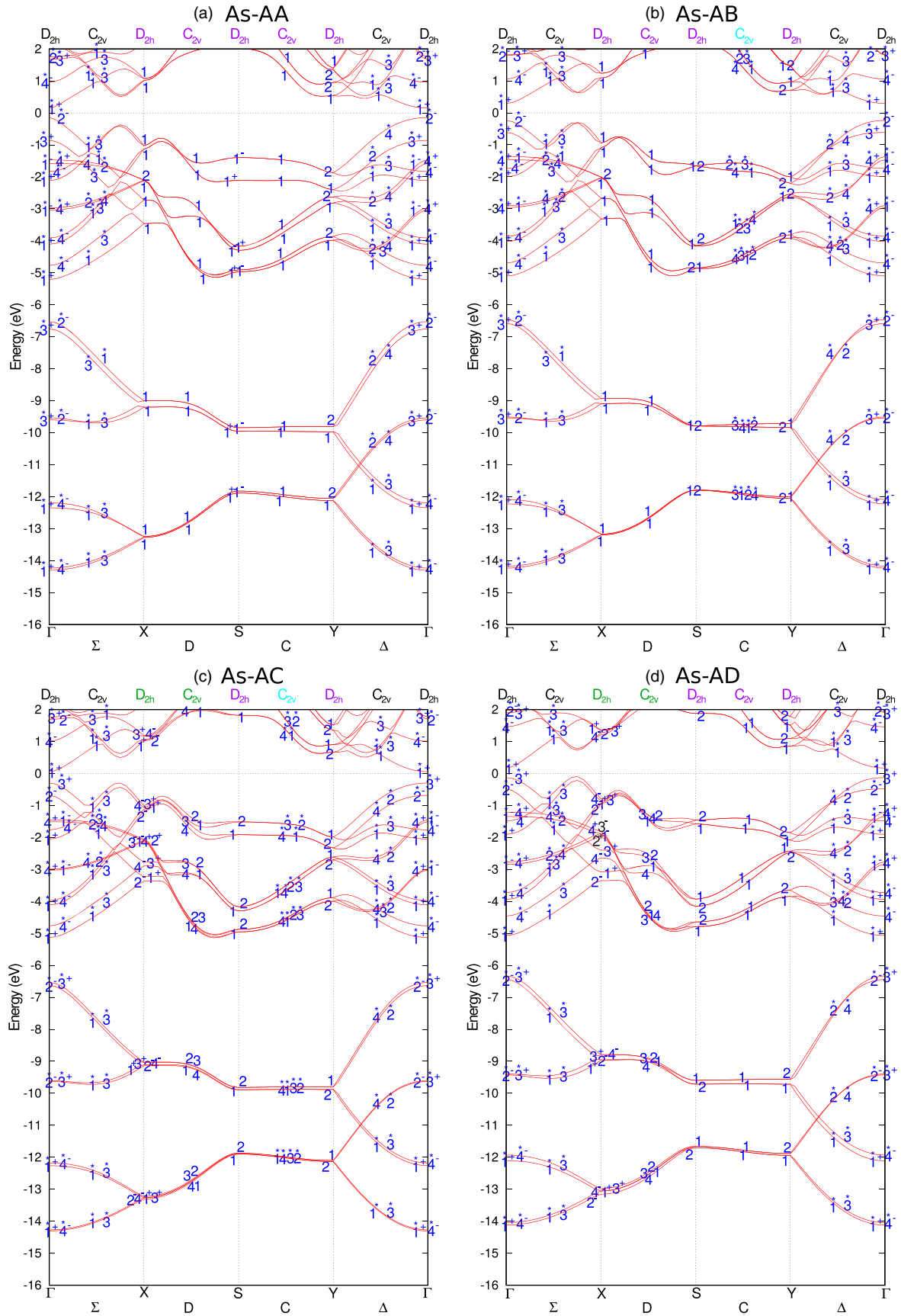
Fig. 4. (Color online) Band structures of bilayer arsenene forming (a) AA, (b) AB, (c) AC and (d) AD stacking structures. Conventional IR are denoted by stars (*) and the nonconventional IR are represented without using stars. The characters of these IR are tabulated in Tables III and IV.
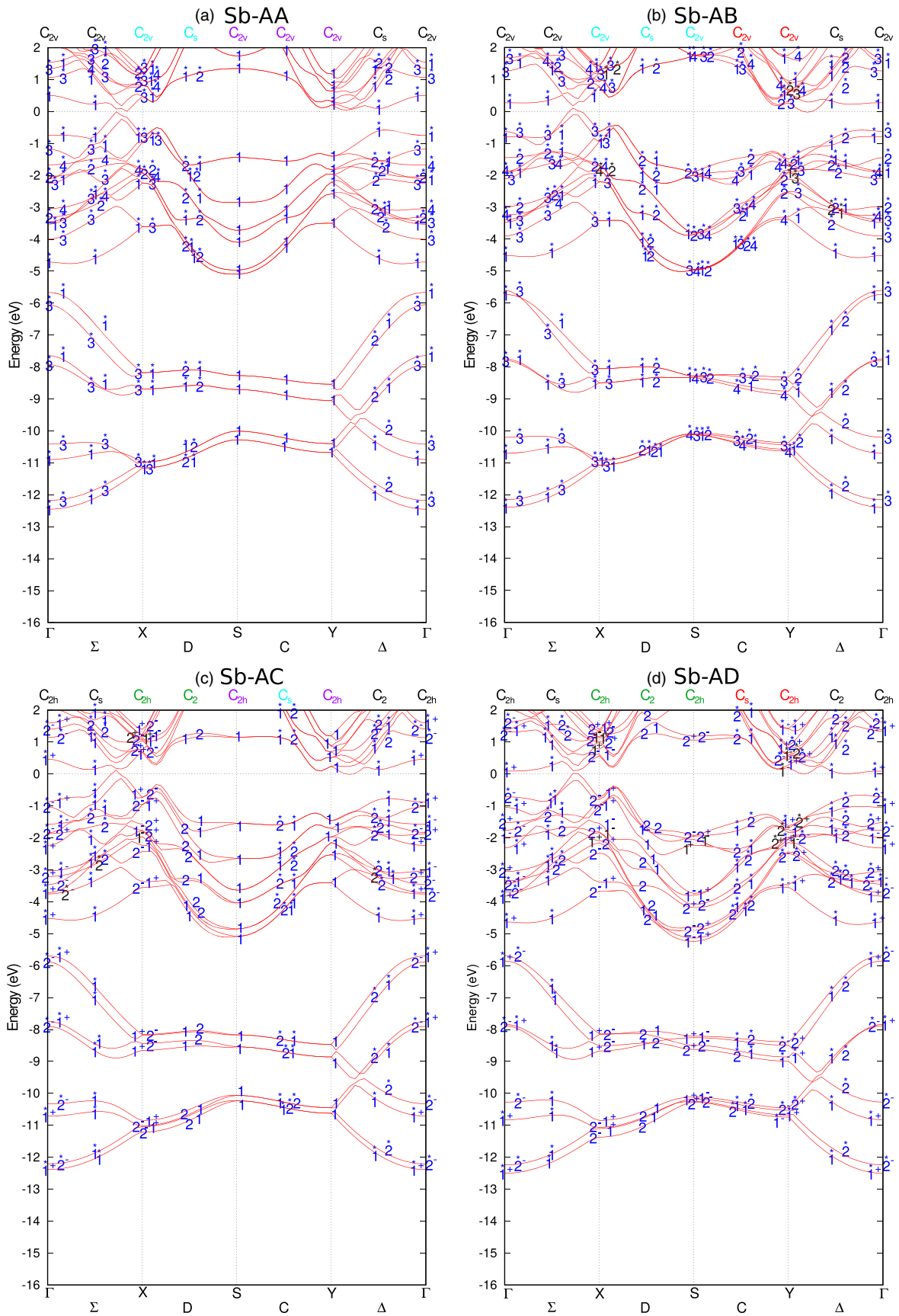
Fig. 5. (Color online) Band structures of bilayer antimonene forming (a) AA, (b) AB, (c) AC and (d) AD stacking structures. Conventional IR are denoted by stars (*) and the nonconventional IR are represented without using stars. The characters of these IR are tabulated in Tables III and V.

the degeneracy among the four stacking structures originates from different space groups.

ORCID iDs

Muhammad Yusuf Hakim Widianto 🔟 https://orcid.org/0000-0002-1720-9754

1) B. Liu and K. Zhou, Prog. Mater. Sci. **100**, 99 (2019).
2) H. Liu, A. T. Neal, Z. Zhu, Z. Luo, X. Xu, D. Tomanek, and P. D. Ye, ACS Nano **8**, 4033 (2014).
3) H. Kaur, S. Yadav, A. K. Srivastava, N. Singh, J. J. Schneider, O. P. Sinha, V. V. Agrawal, and R. Srivastava, Sci. Rep. **6**, 34095 (2016).
4) S. Cahangirov, M. Topsakal, E. Aktürk, H. Sahin, and S. Ciraci, Phys. Rev. Lett. **102**, 236804 (2009).
5) P. Vogt, P. D. Padova, S. Quaresima, J. Avila, E. Frantzeskakis, M. C. Asensio, A. Resta, B. Ealet, and G. L. Lay, Phys. Rev. Lett. **108**, 155501 (2012).
6) S. Huang, W. Kang, and L. Yang, Appl. Phys. Lett. **102**, 133106 (2013).
7) E. Bianco, S. Butler, S. Jiang, O. D. Restrepo, W. Windi, and J. E. Goldberger, ACS Nano **7**, 4414 (2013).
8) K. S. Novoselov, A. K. Geim, S. V. Morozov, D. Jiang, Y. Zhang, S. V. Dubonos, I. V. Grigorieva, and A. A. Firsov, Science **306**, 666 (2004).
9) L. Li, Y. Yu, G. J. Ye, Q. Ge, X. Ou, H. Wu, D. Feng, X. H. Chen, and Y. Zhang, Nat. Nanotechnol. **9**, 372 (2014).
10) Y. Nakanishi et al., Nano Res. **10**, 718 (2017).
11) M. N. Brunetti, O. L. Berman, and R. Y. Kezerashvili, Phys. Rev. B **100**, 155433 (2019).
12) Y. Tanaka, M. Saito, and F. Ishii, Jpn. J. Appl. Phys. **57**, 125201 (2018).
13) M. Saito, Y. Takemori, T. Hashi, T. Nagao, and S. Yaginuma, Jpn. J. Appl. Phys. **46**, 7824 (2007).
14) B. Deng et al., Nat. Commun. **8**, 14474 (2017).
15) Z. Guo et al., Adv. Funct. Mater. **25**, 6996 (2015).
16) C. Kamal and M. Ezawa, Phys. Rev. B **91**, 085423 (2015).
17) M. Pumera and Z. Sofer, Adv. Mater. **29**, 1605299 (2017).
18) S. Sharma, S. Kumar, and U. Schwingenschlögl, Phys. Rev. Appl. **8**, 044013 (2017).
19) N. A. P. Namari and M. Saito, Jpn. J. Appl. Phys. **58**, 061003 (2019).
20) O. Ü. Aktürk, V. O. Özçelik, and S. Ciraci, Phys. Rev. B **91**, 235446 (2015).
21) M. F. Deschênes, O. Waller, T. O. Menteş, A. Locatelli, S. Mukherjee, F. Genuzio, P. L. Levesque, A. Hébert, R. Martel, and O. Moutanabbir, Nano Lett. **17**, 4970 (2017).
22) P. Ares, J. J. Palacios, G. Abellán, J. G. Herrero, and F. Zamora, Adv. Mater. **30**, 1703771 (2017).
23) E. Aktürk, O. Ü. Aktürk, and S. Ciraci, Phys. Rev. B **94**, 014115 (2016).
24) T. Nagao, J. T. Sadowski, M. Saito, S. Yaginuma, Y. Fujikawa, T. Kogure, T. Ohno, Y. Hasegawa, S. Hasegawa, and T. Sakurai, Phys. Rev. Lett. **93**, 105501 (2004).
25) M. Saito, T. Ohno, and T. Miyazaki, Appl. Surf. Sci. **237**, 80 (2004).
26) J. P. Perdew and Y. Wang, Phys. Rev. B **45**, 13244 (1992).
27) J. P. Perdew, K. Burke, and M. Ernzerhof, Phys. Rev. Lett. **77**, 3865 (1996).
28) D. Vanderbilt, Phys. Rev. B **41**, 7892 (1990).
29) N. Troullier and J. L. Martins, Phys. Rev. B **43**, 1993 (1991).
30) S. Minami, I. Sugita, R. Tomita, H. Oshima, and M. Saito, Jpn. J. Appl. Phys. **56**, 105102 (2017).
31) A. Zaharo, A. Purqon, T. Winata, and M. Saito, Jpn. J. Appl. Phys. **59**, 071006 (2020).
32) M. Y. H. Widianto, H. P. Kadarisman, A. M. Yatmeidhy, and M. Saito, Jpn. J. Appl. Phys. **59**, 071001 (2020).
33) T. Ohno, T. Yamamoto, T. Kokubo, A. Azami, Y. Sakaguchi, T. Uda, T. Yamasaki, D. Fukata, and J. Koga, SC '07: Proc. 2007 ACM/IEEE Conf. on Supercomputing, 2007, Article 57.
34) R. S. Mulliken, J. Chem. Phys. **23**, 1997 (1955).
35) R. S. Mulliken, J. Chem. Phys. **24**, 1118 (1956).
36) T. Zhang, J.-H. Lin, Y.-M. Yu, X.-R. Chen, and W.-M. Liu, Sci. Rep. **5**, 13927 (2015).
37) K. Mi, J. Xie, M. S. Si, and C. X. Gao, Europhys. Lett. **117**, 27002 (2017).
38) G. Wang, R. Pandey, and S. P. Karna, Appl. Mater. Interfaces **7**, 11490 (2015).
39) M. Xie, Z. Zhang, B. Cai, Y. Gu, X. Liu, E. Kan, and H. Zeng, Nano Energy **38**, 561 (2017).
40) Z.-Q. Shi et al., Nano Lett. **20**, 8408 (2020).